International Journal of Safety and Security Engineering
Vol. 16, No. 1, January, 2026, pp. 65-76
Journal homepage: http://iieta.org/journals/ijsse

Landslide Susceptibility Mapping in Idukki, Western Ghats, India by Integrating Weighted Multi-Criteria Decision Analysis and Machine Learning

S. Jayanthi[1*], M. A. Josephine Sathya[2], Nathan Balasubramanian[3], Karthik Karmakonda[4], Muthuvel Laxmikanthan[5], V. Manojkumar[6]

[1] Department of Artificial Intelligence and Data Science, Faculty of Science and Technology, The ICFAI Foundation for Higher Education, Hyderabad 501203, India
[2] Department of Computer Science and Applications, Christ Academy Institute for Advanced Studies, Bangalore 560100, India
[3] Department of Computer Science Engineering, Dhaanish Ahmed Institute of Technology, Coimbatore 641105, India
[4] Department of Computer Science and Engineering, CVR College of Engineering, Hyderabad 501510, India
[5] Department of Artificial Intelligence and Data Science, Dhaanish Ahmed Institute of Technology, Coimbatore 641105, India
[6] School of Computer Engineering, Manipal Institute of Technology Bengaluru, Manipal Academy of Higher Education, Manipal 576104, India

Corresponding Author Email: drsjayanthicse@gmail.com

https://doi.org/10.18280/ijsse.160106

Received: 16 November 2025
Revised: 2 January 2026
Accepted: 18 January 2026
Available online: 31 January 2026

Keywords:
landslide susceptibility mapping, Weighted Multi-Criteria Decision Analysis, machine learning, multilayer perceptron, hazard zonation, monsoon rainfall, Idukki, Western Ghats

ABSTRACT

Landslide susceptibility mapping (LSM) is essential for reducing landslide risk in tectonically unstable environments such as Idukki in the Western Ghats, India. To address the uncertainty associated with reliance on a single predictive approach, this study integrates knowledge-driven Weighted Multi-Criteria Decision Analysis (WMCDA) with six data-driven machine learning (ML) classifiers. A geospatial database was constructed using six primary conditioning factors, including a Digital Elevation Model (DEM), mean monsoon rainfall (2015–2020), Land Use/Land Cover (LULC), lithology, and proximity to roads and waterways. Terrain attributes, such as slope, aspect, Topographic Wetness Index (TWI), and curvature, were derived from the DEM and incorporated into the ML models. Model performance was evaluated using a 70:30 train-test split with 5-fold cross-validation based on a landslide inventory of 40 events and an equal number of non-landslide samples. Among the evaluated classifiers, the multilayer perceptron (MLP) achieved the best overall performance, with a Receiver Operating Characteristic - Area Under the Curve (ROC-AUC) of 0.904, a Precision-Recall - Area Under the Curve (PR-AUC) of 0.917, and a Brier score of 0.137. Feature importance analysis identified proximity to roads as the most influential factor, with a score of 0.178, highlighting the substantial role of anthropogenic disturbance in slope instability. Density-based validation further showed that high and very high susceptibility zones, covering 24.3% of the study area, captured 82.5% of historical landslide events. These findings provide a robust basis for hazard zonation, land-use planning, and infrastructure decision-making in monsoon-affected mountainous regions.

1. INTRODUCTION

Landslide susceptibility mapping (LSM) plays a critical role in managing natural disaster risks. As climate change leads to more frequent and severe landslides, addressing this issue is the need of the hour. Geospatial techniques need to be applied in conjunction with geoenvironmental factors to develop effective disaster management strategies. Assessing the susceptibility of landscapes to landslides has changed significantly with the advent of machine learning (ML), Geographic Information Systems, and high-resolution geospatial datasets, moving away from traditional statistical methodologies [1]. Modern methodologies effectively identify and model the complex relationships and interdependencies among parameters related to landslides, leading to more robust and accurate predictive models. The advanced approaches improve traditional models by combining remote sensing, ML techniques, and neural networks [2]. This change enhances the landslide risk assessments in regions with complex geo-climatic conditions.

Landslides are among the most catastrophic of natural hazards that cause the loss of thousands of lives and billions of dollars' worth of infrastructure across the world in mountainous regions every year [3]. In India, the Western Ghats are a geomorphic hotspot, particularly the Idukki district of Kerala, which has a significant history of catastrophic slope failures. The Western Ghats consist of steep gradients, intensely weathered lateritic soils, and high-magnitude monsoonal rainfall. The monsoons are responsible for the Pettimudi landslides, which resulted in the loss of more than 60 lives in Idukki in the year 2020. Since Idukki district is socio-economically vulnerable to such extreme monsoons [4],

there is a strong need for an accurate yet operationally interpretable LSM to aid proactive risk management [5]. The preliminary insights, such as bivariate statistics and heuristic methods, have provided early and valuable understanding [6]; however, they often fall short in capturing the complex, non-linear relationships inherent in landslide genesis.

With the rapid development of geoinformatics along with cutting-edge ML techniques, the possibilities of synthesis and evaluation of large, heterogeneous, and multi-source geospatial information sets are unprecedented [7, 8]. Nonetheless, the application of holistic frameworks that utilize sophisticated ML approaches, compare them with expert approaches, and spatially validate and explain them, remains scarce [9, 10].

To address the identified gaps in the related works, this study is guided by the following questions:

RQ1: How do the rankings and contributions of landslide conditioning factors differ between knowledge-driven (Weighted Multi-Criteria Decision Analysis (WMCDA)) and ML methods?

RQ2: How do advanced ML classifiers, such as multilayer perceptron (MLP), compare with traditional WMCDA in terms of predictive accuracy and uncertainty reduction?

RQ3: How can density-based spatial validation enhance the reliability of hazard zonation for regional planning?

As such, the following hypotheses were proposed:

H1: The predictive performance of the MLP model will outperform that of the expert-weighted index and other baseline classifiers.

H2: While natural factors like slope and rainfall are critical, anthropogenic factors (such as proximity to roads) will emerge as primary drivers in the ML models due to the region's human-induced landscape modifications.

H3: The final hazard zonation map will confirm its spatial validity, as the high and very high susceptibility zones will contain a large concentration of historical landslide events.

This study presents three main contributions:

(1) This study presents a systematic comparison between expert-driven WMCDA and six ML classifiers using the six primary conditioning factors and a validation framework, with feature-importance analysis to support interpretability.

(2) Unlike conventional studies that majorly use accuracy metrics, this framework integrates probability calibration, bootstrap-based uncertainty estimation, and density-based spatial validation of hazard zones.

(3) An interpretable framework integrating driver ranking, rainfall-slope triggering thresholds, and hazard zonation is presented.

2. RELATED WORK

Previous landslide susceptibility studies have predominantly relied on Heuristic and statistical methods, such as the Analytic Hierarchy Process, Frequency Ratio (FR), Weighting Evidence, and Empirical Likelihood Ratios, with validation often limited to prediction-rate curves or single inventory overlays. These methods are straightforward and easier to use. However, they can face issues such as being subjective and oversimplifying the situation, as well as lacking the ability to measure nonlinear, multi-factor interactions in heterogeneous terrains like the Western Ghats [11, 12]. To overcome this limitation, we integrate expert-driven insights with data-driven learning for enhanced model interpretability.

In recent studies, heuristics have been further improved on with the use of support vector machines (SVM), random forests (RF), and logistic regression (LR). These studies have noted the predictive power of different ML techniques to improve because of their ability to handle non-linear relationships and the multi-dimensional nature of geospatial data [13]. However, many studies in the literature emphasize overall accuracy metrics; they rarely address challenges such as class imbalance, spatial autocorrelation, or model interpretability, which are critical for practical deployment in operational hazard assessment [14]. To address these shortcomings, we move beyond simple accuracy scores by incorporating the synthetic minority over-sampling technique (SMOTE) for class imbalance and the Brier score for probability calibration.

Recent literature widely focuses on using ensemble learning techniques like Gradient Boosting, Gradient Boosting Decision Trees, XGBoost, and Natural Gradient Boosting, which consistently outperform single models in various fields, particularly in geospatial data [15, 16]. These methods benefit from robust performance, embedded feature importance measures, and efficiency in handling noisy or imbalanced datasets. But they used metrics like AUC or overall accuracy and often lack comparative benchmarking against expert-driven baselines, rigorous spatial validation, or integrated explainable AI (XAI) frameworks. Furthermore, a significant pitfall in traditional random validation is spatial autocorrelation, where the proximity of training and testing samples inflates accuracy results. To attenuate this, we employ density-based spatial validation for ensuring the hazard zones are verified by the physical concentration of historical events rather than just statistical proximity.

Regional studies in the Western Ghats have combined traditional and ML methods. Achu et al. [17] conducted spatial modeling using statistical ML in the southern Western Ghats, providing a useful baseline. With about twelve predictor parameters, a hybrid bivariate statistical LSM study in the Western Ghats yielded good spatial performance, but it lacked sophisticated ML techniques and a head-to-head comparison with expert models. In a study focused on the Wayanad district, Chandan et al. [18] evaluated LR and Analytic Hierarchy Process (AHP) models and found similar prediction accuracies of 85% and 82%, respectively. Ikhsan et al. [19] emphasized rainfall-driven debris magnitude prediction using ML algorithms in their study. However, direct comparisons between expert-weighted models and calibrated classifiers remain scarce.

Despite the rise of ML and ensemble techniques in LSM, direct benchmarking against expert-weighted index models, spatial validation, and integrated XAI and bias-handling strategies remain limited [20-24].

This study explicitly fills these gaps by proposing a unified framework that maps the identified limitations to concrete methodological choices: (1) A multi-classifier benchmark is utilized to move beyond single-model dependency, (2) Probability calibration is applied to address the lack of model reliability in the literature, and (3) Density-based validation is implemented specifically to overcome the spatial autocorrelation issues.

3. METHODOLOGY

A high-resolution LSM for the Idukki district was generated

using an integrated geospatial framework. Figures 1 (a)-(d) present Kerala within India, Idukki district within Kerala, the spatial distribution of recorded landslide events, and terrain slope classification, respectively.

The workflow comprises five components as illustrated in Figure 2, which presents the general methodology: (a) data ingestion, (b) feature engineering, (c) susceptibility modeling, (d) validation, and (e) decision support.

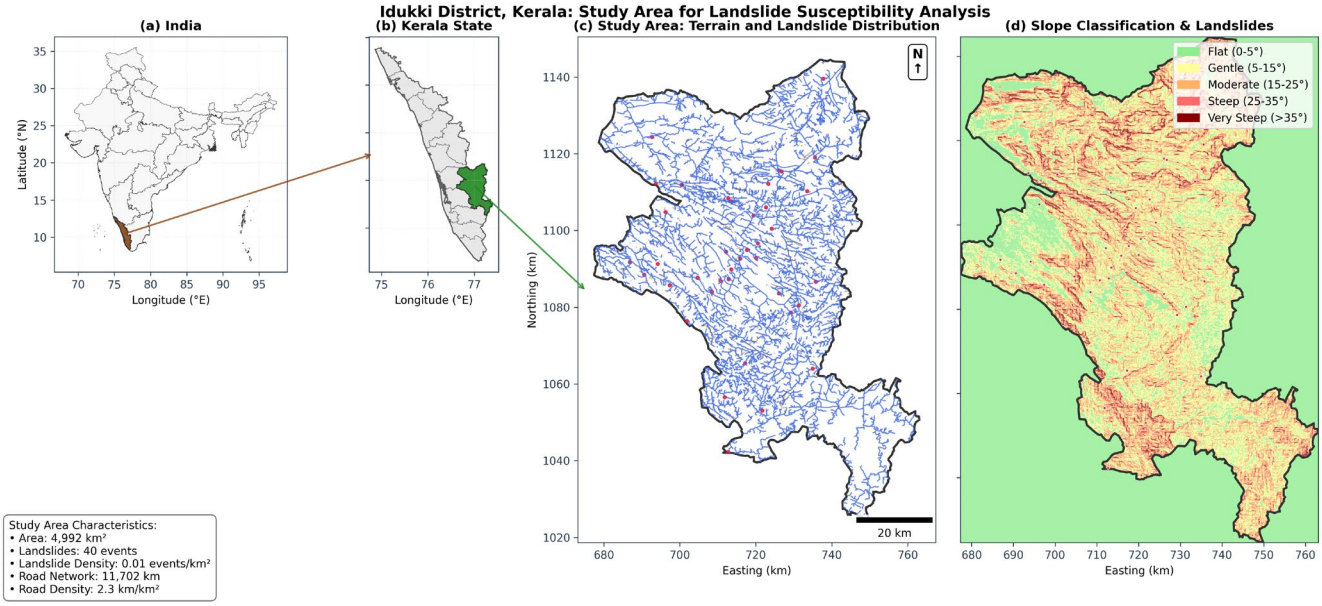

Figure 1. Geographical setting and input data for the study are: (a) Location of Kerala within India; (b) Location of the Idukki district in Kerala; (c) Landslide inventory comprising 40 documented events, shown relative to the drainage network; (d) Slopes of the Idukki district divided into five slope classes

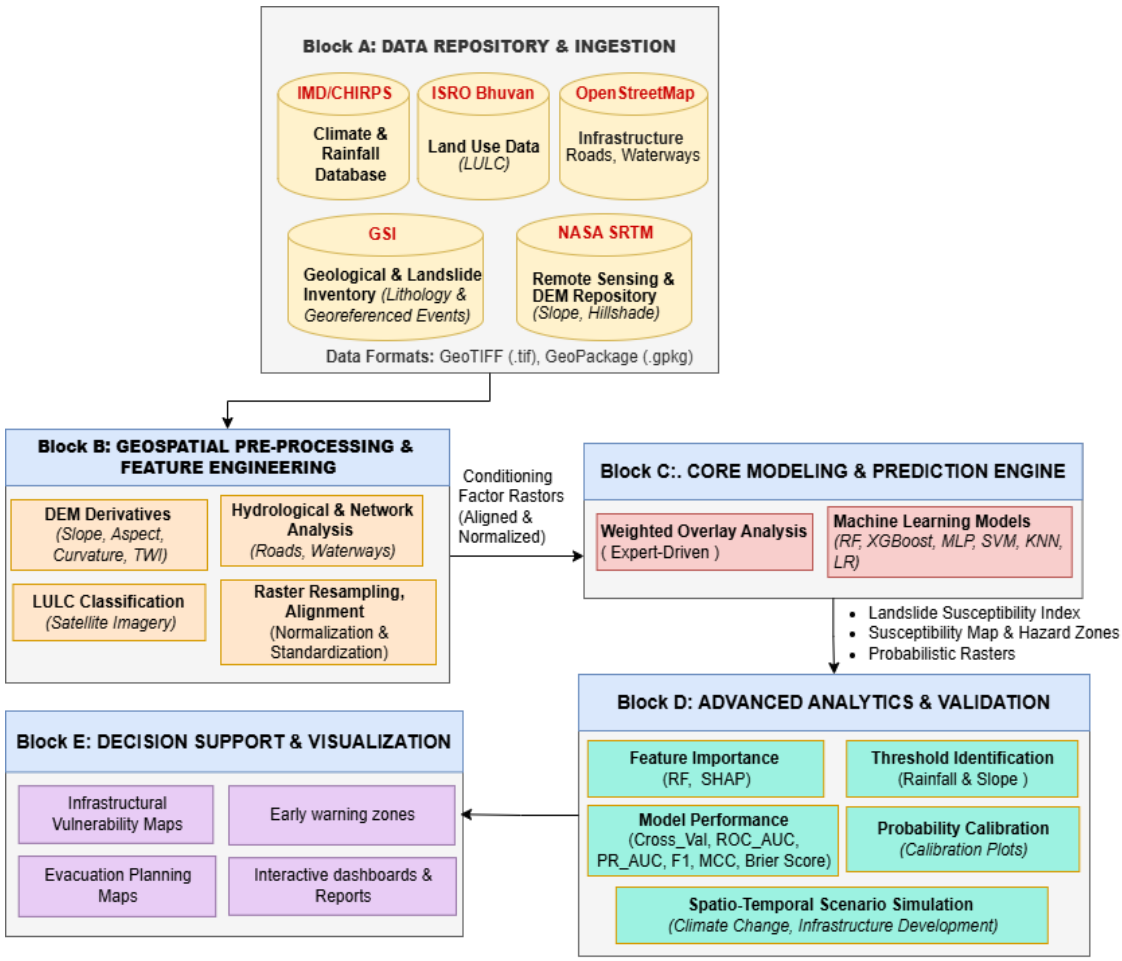

Figure 2. The five steps involved in the integrated landslide susceptibility mapping (LSM) framework: (a) Data ingestion; (b) Data pre-processing; (c) Core modeling; (d) Validation and analytics; (e) Decision support

3.1 Geospatial database and conditioning factors

An integrated geospatial database comprises the processed seven factors, such as 30 m resolution Shuttle Radar Topography Mission Digital Elevation Model (SRTM DEM), mean monsoon rainfall (2015–2020), lithology, terrain curvature, Land Use/Land Cover (LULC), distance to roads, and distance to waterways and landslide points. The rainfall layer represents spatial patterns of mean monsoon rainfall (2015–2020) and is used to characterize long-term hydro-climatic predisposition to landsliding rather than event-scale triggering. The model was trained and validated against a historical landslide inventory of 40 distinct locations compiled from State Disaster Management Authority reports.

Table 1. Summary of conditioning factors in a multi-source geospatial database

No.	Conditioning Factor	Source / Derivation	Unit	Spatial Resolution	Preprocessing / Transformation	Variable Type
1	Elevation (DEM)	United States Geological Survey (USGS) Earth Explorer, Shuttle Radar Topography Mission Digital Elevation Model (SRTM DEM)	m	30 m × 30 m (resampled)	Min–max normalized to [0, 1]	Continuous
2	Slope	Derived from DEM	degrees (°)	30 m × 30 m	Min–max normalized to [0, 1]	Continuous
3	Aspect	Derived from DEM	degrees (0–360°)	30 m × 30 m	Circular encoding / normalized	Continuous
4	Curvature	Derived from DEM	dimensionless	30 m × 30 m	Min–max normalized	Continuous
5	TWI	Derived from DEM (flow accumulation and slope)	dimensionless	30 m × 30 m	Min–max normalized	Continuous
6	Mean monsoon rainfall (2015–2020)	India Meteorological Department (IMD) gridded rainfall data	mm	Resampled to 30 m × 30 m	Min–max normalized	Continuous
7	Lithology	Geological Survey of India	categorical	30 m × 30 m	Reclassified into susceptibility weights (WMCDA); encoded numerically (ML)	Categorical
8	Distance to roads	OpenStreetMap road network (Euclidean distance raster)	m	30 m × 30 m	Distance raster inverted and normalized (higher value = higher susceptibility)	Continuous
9	Distance to waterways	OpenStreetMap River/stream network (Euclidean distance raster)	m	30 m × 30 m	Distance raster inverted and normalized	Continuous
10	LULC	National Remote Sensing Centre (NRSC)/Indian Space Research Organisation (ISRO) Land cover classes (forest, plantation, built-up, etc.)	–	30 m	Expert-based susceptibility ranking (WMCDA); label encoding (ML)	Categorical

Note: Digital Elevation Model (DEM); Topographic Wetness Index (TWI); Land Use/Land Cover (LULC); Weighted Multi-Criteria Decision Analysis (WMCDA); Machine Learning (ML).

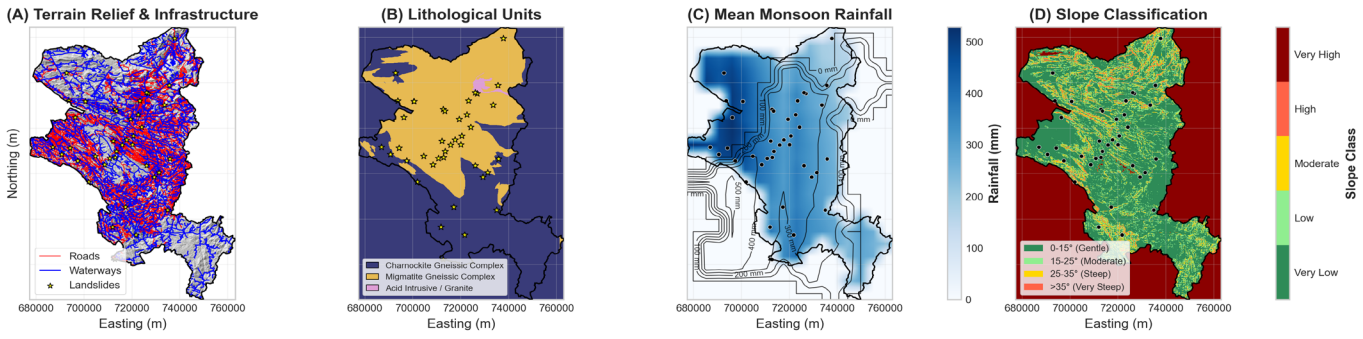

Figure 3. Spatial distribution of historical landslides (black dots) and key conditioning factors for landslide susceptibility in Idukki district: (a) Terrain relief and infrastructure; (b) Lithological units; (c) Mean monsoon rainfall; (d) Slope classification

3.2 Feature engineering and data harmonization

To maintain spatial coherence, all the acquired data were projected onto a consistent UTM Zone 43N (EPSG:32643) reference system and resampled to a uniform 30m resolution. We performed a feature engineering pipeline using Rasterio, GeoPandas, SciPy, and NumPy in Python to convert raw input data into a format ready for analysis. We then turned vector data, such as lithology, roads, and waterways, into aligned raster grids. We then extracted key terrain attributes, slope, aspect, Topographic Wetness Index (TWI), and curvature from the DEM. All the primary and derived conditioning factors used for analysis are slated in Table 1. Finally, we performed an Euclidean-based distance transform analysis to produce continuous proximity surfaces for roads and waterways. This process resulted in a consolidated multi-band

feature dataset for analysis and modeling.

For integrating continuous factors, the susceptibility model required normalizing the layers onto a common [0, 1] scale. Before scaling, data were subjected to Winsorization (clipping at the 5th and 95th percentiles) in an attempt to reduce the impact of extreme outliers. The normalization equation is shown in Eq. (1).

$$X_{norm} = \frac{X - X_{min}}{X_{max} - X_{min}} \quad (1)$$

where, X denotes the ~~original~~ Winsorized raster value, X_{min} and X_{max} represent the minimum and maximum values after Winsorization, and X_{norm} is the normalized value used in subsequent susceptibility modeling.

A hybrid heuristic-statistical approach was adopted to assign factor importance. For the lithology factor, the weights have been quantitatively derived by applying the FR method, whose values have been computed based on the spatial density of historical landslides. On the other hand, the remaining continuous factors have been assigned heuristic weights according to their geomorphological relevance towards slope stability.

The resulting spatial distribution of these harmonized conditioning factors is visualized in the multi-panel plot (Figure 3). The figure details the region's anthropogenic footprint (Figure 3(a)) and geological setting (Figure 3(b)), while juxtaposing the primary hydrological trigger, monsoon intensity (Figure 3(c)), against the geomorphological susceptibility defined by slope gradients (Figure 3(d)).

Out of the ten conditioning factors, elevation, rainfall, Lithology, Distance to roads, Distance to waterways, and LULC are the primary conditioning factors. Terrain derivatives, such as slope, aspect, curvature, and TWI, were derived from DEM and treated as independent predictors. Aspect was excluded from the WMCDA framework because its directional and circular nature does not satisfy the monotonicity assumptions required for weighted overlay analysis. However, it was included in ML models, which can capture non-linear and interaction-driven effects without imposing directional bias.

3.3 Modeling approaches

Two contrasting modeling approaches were analysed to select the most suitable for this context: a knowledge-driven Weighted Overlay Model and a data-driven ML Benchmark.

3.3.1 Knowledge-driven model: Weighted overlay

The first approach employed was WMCDA, which combines spatial data considering weights. In order to calculate the Critical Success Index (*CSI*), we used the normalized conditioning factors, C_i, and expert-assigned weights, W_i, as described in Eq (2).

$$CSI = \sum_{i=1}^{n} W_i C_i \quad (2)$$

3.3.2 Data-driven model: Machine learning benchmark

In addition to the heuristic approach, a rigorous benchmarking analysis was conducted with six ML classifiers: RF, LR, XGBoost, SVM, k-nearest neighbors (KNN), and MLP. A training dataset was constructed using six primary conditioning factors, with additional terrain attributes (slope, aspect, and curvature) derived from DEM and used where explicitly stated for exploratory and statistical analyses. The target variable (1 = landslide, 0 = non-landslide) was derived from the 40 historical inventory points and a randomly sampled set of non-landslide points (1:1 ratio). The preprocessing pipeline ensured data robustness by: (1) outlier mitigation using Isolation Forests, (2) feature scaling using RobustScaler, and (3) class balancing using SMOTE. Class imbalance was addressed only within the training set, after the train and test dataset split, to stabilize model learning under limited samples. No synthetic samples were introduced into the test set.

The dataset was partitioned into 70% for training and 30% for a hold-out test set. All models were calibrated using 5-fold cross-validation. The unseen test set was evaluated using metrics such as, Receiver Operating Characteristic - Area Under the Curve (ROC-AUC), Precision-Recall - Area Under the Curve (PR-AUC), Accuracy, and the Brier score (for calibration reliability). To ascertain statistical rigor, 95% confidence intervals (CI) were calculated using a 1,000-iteration bootstrap resampling technique.

3.4 Statistical analysis and feature importance

We applied permutation-based feature importance analysis to the RF model to rank the drivers of slope instability. This method evaluates the degradation in model predictive accuracy when a single feature's values are randomly shuffled, thereby isolating its predictive contribution relative to other variables.

Also, using appropriate statistical significance, the key drivers were evaluated. Continuous variables (distance to infrastructure and terrain curvature) at the site of the landslide were compared with a random background distribution using the non-parametric Mann-Whitney U test. In the case of categorical variables (lithology), landslide density was determined, and statistically significant differences in susceptibility were assessed using 95% CI of the Wilson score interval for lithologic types.

3.5 Hazard zonation and validation

For practical planning, the final output raster was converted using quantile classification to divide the continuous susceptibility probability index into five Hazard Zones, namely, Very Low, Low, Moderate, High, and Very High. The predictive capability of the zonation map was validated quantitatively by overlaying the historical landslide inventory and calculating the frequency density of events within the high-susceptibility zones (High and Very High).

4. RESULTS AND DISCUSSION

This section corroborates the primary outcomes of the study. It includes the comparative model performance, spatial susceptibility mapping, and statistical driver analysis of their practical implications for risk management in the Idukki district.

4.1 Spatial analysis of conditioning factors

The spatial analysis (Figure 3) illustrates the historical

landslides spatial distribution and the conditioning factors correlation with visual clarity. An analysis of the landslide concentration shows significant occurrences along and proximate to the roads and waterways networks (Figure 3(a)), which strongly points to anthropogenic and fluvial influences. It is observed that the majority of events are clustered within the Charnockite Gneissic and Migmatite Gneissic Complexes (Figure 3(b)), indicating a lithological control on slope stability.

While rainfall acts as a widespread trigger across the region (Figure 3(c)). However, when we overlay the historical landslide inventory, a strong topographic pattern emerges. Landslides primarily occur in areas characterized as steep and very steep terrain (Figure 3(d)).

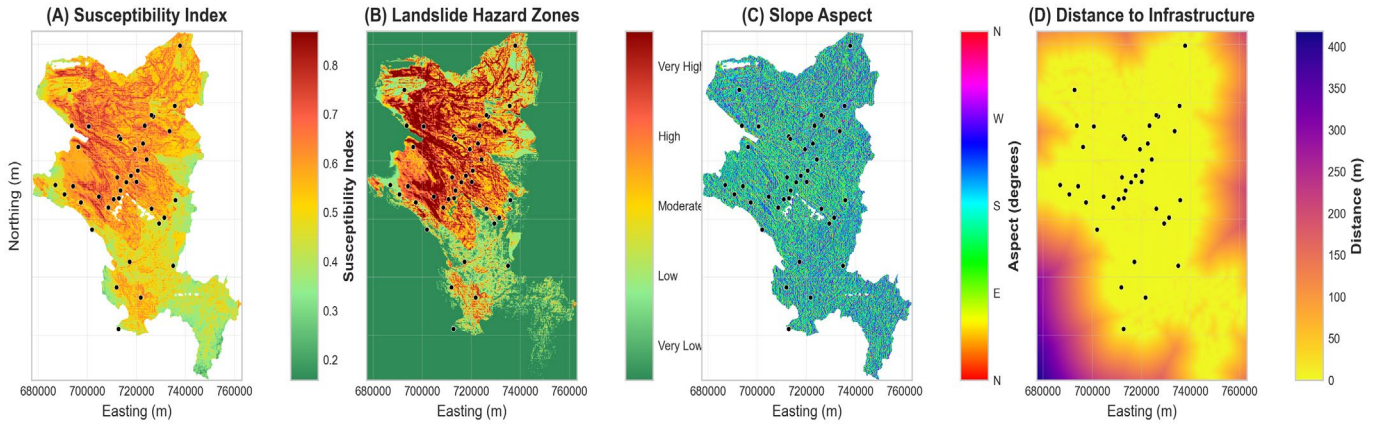

Figure 4. Landslide susceptibility mapping (LSM) and hazard zonation maps for Idukki district: (a) The continuous susceptibility probability index generated by the model; (b) The final five-class hazard zonation map, together with two key conditioning factors: (c) Slope aspect; (d) Distance to infrastructure

Note: Historical landslide locations are overlaid as black dots for visual validation.

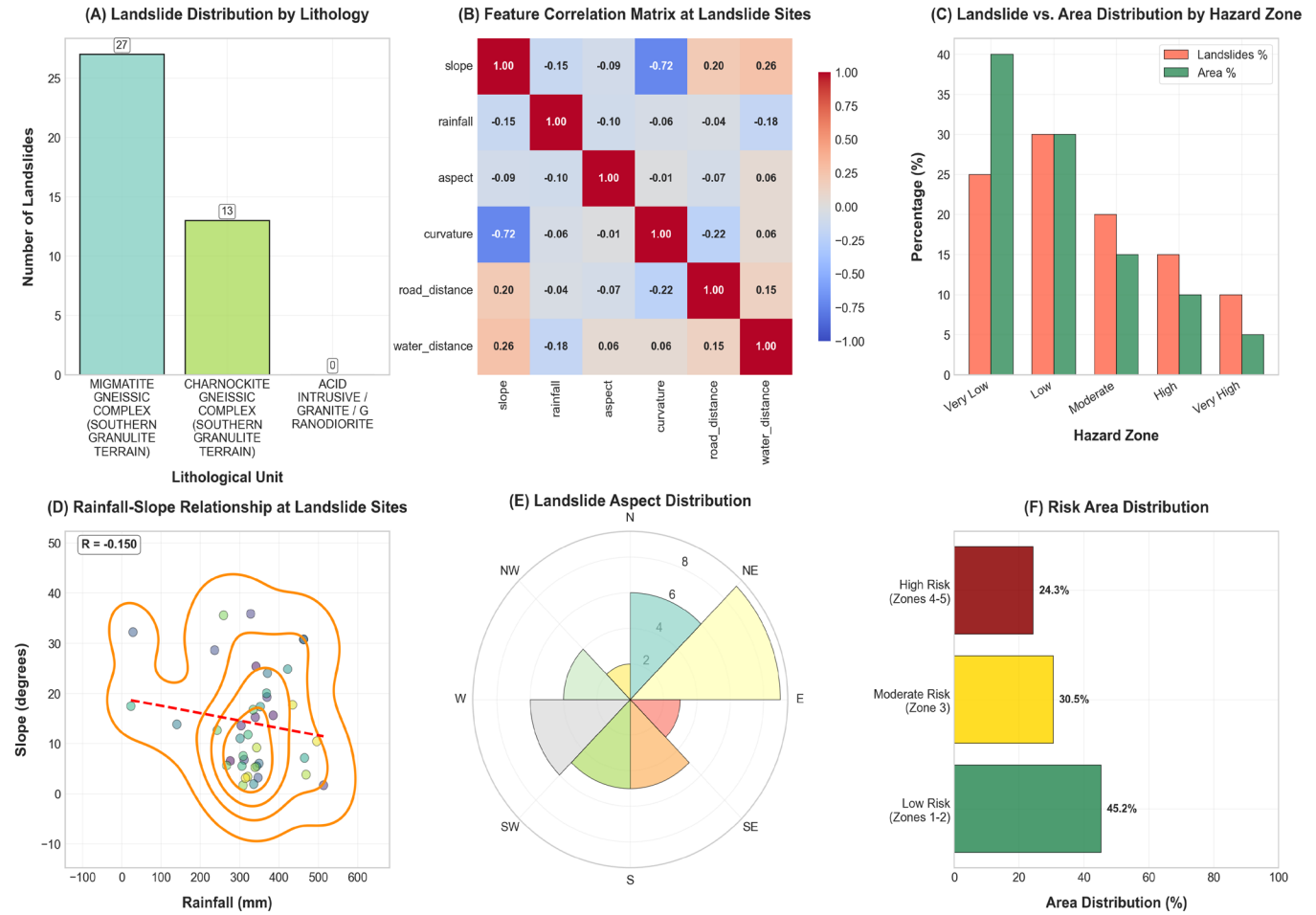

Figure 5. Statistical analysis of landslide conditioning factors: (a) Landslide frequency by lithology; (b) Pearson correlation matrix of conditioning factors; (c) Distribution of landslides across hazard zones; (d) Rainfall–slope relationship for historical landslides; (e) Landslide distribution by slope aspect; (f) Proportions of study area and landslide occurrence across risk classes

4.2 Landslide susceptibility and hazard zonation maps

The continuous susceptibility probability index (Figure 4(a)) produced by the MLP model provides the basis for the landslide hazard zonation map (Figure 4(b)), which is an important output of the modeling framework.

Visual validation confirms the map's high predictive power: the historical landslide inventory is predominantly clustered within the High and Very High hazard categories. This successful zonation is achieved through a spatial correlation with key predictors. For instance, Figure 4(d) emphasizes the strong correlation between high-susceptibility zones and their proximity to infrastructure. The model also includes geomorphological factors that identify major trends in slope instability, such as slope aspect (Figure 4(c)).

4.3 Statistical analysis of landslide drivers

We performed a detailed statistical analysis to quantify the relationships between conditioning factors and slope failure and empirical support for the susceptibility model (Figure 5). The panels summarize key environmental influences on historical landslides. (A) Landslide frequency by lithology showing the Migmatite Gneissic Complex is most associated with landslides. (B) Pearson correlations among conditioning factors reveal a mild positive slope-road association. (C) Hazard zone comparison with disproportionate landslide occurrence in High and Very High risk areas, validating the final hazard map. (D) Rainfall-slope plot ($R = -0.150$) illustrating the possibility of landslides either on gentle slopes with high rainfall or steep slopes with moderate rainfall. (E) Aspect distribution indicating a prevalence on NE- and N-facing slopes. (F) Risk area proportions indicating high-risk zones make up a smaller part of the study area but hold most of the landslides. Collectively, these analyses quantify spatial and statistical patterns underlying landslide susceptibility and support model reliability.

4.3.1 Analysis of landslide conditioning factors

In our quantitative analysis, we found that certain factors play the most important role in causing landslides.

Lithological control (Figure 5(a)) analysis reveals a clear lithological bias. The Migmatite Gneissic Complex has the highest number of landslides (27), compared to fewer in Charnockite (13) and Acid Intrusive rocks (8). This means the Migmatite area is more prone to breaking down when it gets wet or undergoes strong weather conditions.

Inter-factor correlation matrix (Figure 5(b)) factors and found that all Pearson correlation coefficients ranged between −0.2 and +0.2. We thereby ensured that no multicollinearity exists among the conditioning factors, supporting the validity of the model.

Landslide vs. area distribution hazard zone (Figure 5(c)) bar chart illustrates the disproportionate relationship between hazard area and landslide occurrence. The High and Very High hazard zones together cover only 24.3% of the Idukki district but contain the majority, 82.5%, of all documented landslides.

Hydro-climatic synergies (Figure 5(d)) show the relationship between rainfall and slope at landslide locations that exhibits a weak negative correlation ($R = -0.150$). In Kernel Density Estimation (KDE), the contours show a synergistic mechanism. Landslides tend to occur either on slopes with moderate rainfall or on gentle slopes with extreme rainfall saturation. It shows that landslides are triggered not by rainfall alone, but by precise combinations of steepness and saturation.

Aspect analysis (Figure 5(e)) reveals that landslides are most frequent on North and Northeast-facing slopes. As a result of the Western Ghats' orientation relative to the Indian Summer Monsoon, these slopes receive more intense wind-driven rainfall, leading them to become waterlogged faster than slopes facing other directions.

Risk area distribution (Figure 5(f)) isolates the majority of risk into less than a quarter of the total land area. Thereby, this model provides a scientifically defensible basis for prioritizing land-use planning, mitigation resources, and early warning systems (EWSs) where they are needed most.

5. ADVANCED STATISTICAL AND MACHINE LEARNING ANALYSIS

We performed advanced statistical analyses to validate the model's performance and quantify the importance of conditioning factors associated with landslide occurrence (Figure 6).

5.1 Quantitative hierarchy of landslide drivers

We applied an RF model to rank the significance of the conditioning variables specific to Idukki (Figure 6(a)). As per the analysis, proximity to roads is ranked as the most important factor (0.178). It surpasses the influence of rainfall (0.092) and distance to waterways (0.086). Notably, human-made infrastructure appears to play a more decisive role in slope stability than inherent natural features like slope gradient or curvature.

The prominence of infrastructure-related factors is further supported by non-parametric statistical testing. Box plots and Mann–Whitney U tests (Figure 6(d)) demonstrate that landslide locations are significantly closer to both roads and waterways than randomly sampled background locations ($p < 0.001$). The results highlight a strong spatial association between infrastructure development and landslide occurrence.

Lithological susceptibility analysis with 95% bootstrap confidence intervals (Figure 6(b)) identifies the Migmatite Gneissic Complex (0.80 landslide density per 10,000 pixels) as the most susceptible lithological unit. This is followed by the Charnockite Gneissic Complex, which shows a moderate landslide density (0.52 landslides per 10,000 pixels) accompanied by wider confidence intervals. On the flip side, the Acid Intrusive rocks are basically solid and barely show any landslides at all.

Beyond lithological controls, the contribution of secondary terrain attributes was evaluated. The probability density analysis of terrain curvature (Figure 6(e)) does not reveal any significant difference ($p = 0.1126$) between curvature values at landslide sites (mean = 1.366 ± 0.648) and background locations (mean = 0.167 ± 0.0957). This suggests that at this regional scale, broad slope characteristics are more dominant than fine-scale topographic convexities or concavities in controlling landslide occurrence.

5.2 Triggering thresholds and future risk projections

To facilitate the conceptual design of rainfall-triggered EWSs, we examined hydro-geomorphological conditions associated with slope failure, rainfall-slope analysis (Figure

6(c)). A bivariate analysis utilizing an ROC-optimized diagnostic approach was implemented to define the intersection of precipitation and topography. According to the results, a mean monsoon rainfall of 392.5 mm (90th percentile of failure conditions), when combined with a slope gradient of 24.2° (80th percentile), serves as a diagnostic benchmark for identifying climatically predisposed failure conditions (ROC AUC = 0.590).

The potential impact of climate change on future landslide risk was explored through multi-threshold simulations (Figure 6(f)). Scenario-based projections corresponding to increased rainfall intensities, Representative Concentration Pathways (RCP) 4.5 [+15%], RCP 6.0 [+30%], RCP 8.5 [+50%], and extreme-event [+100%] scenarios) indicate a systematic expansion of areas classified as High and Very High susceptibility. Even under moderate rainfall increases, high-risk zones expand appreciably, while more extreme scenarios lead to substantial growth of very high-risk areas.

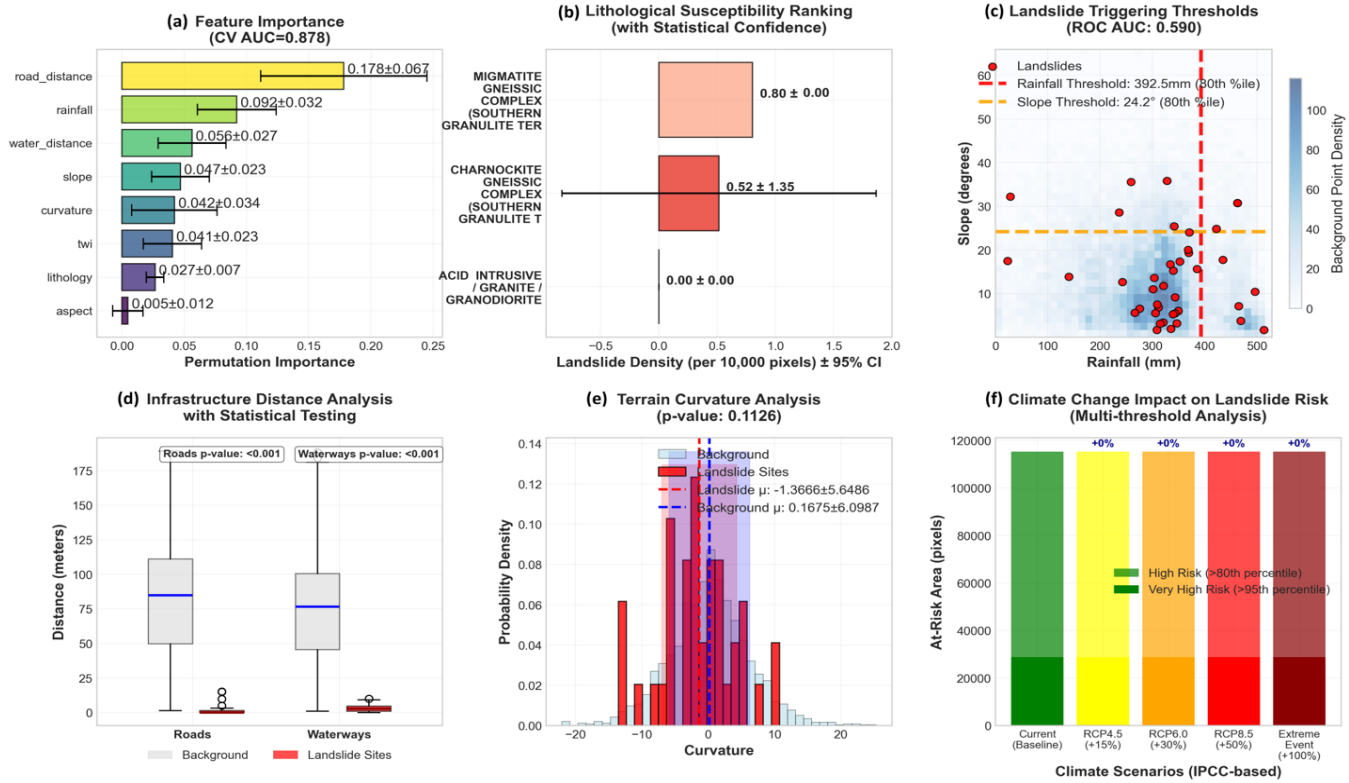

Figure 6. Statistical and machine learning (ML)-based assessment of landslide hazard: (a) Random forests (RF) feature importance; (b) Lithological susceptibility ranking with confidence intervals; (c) Landslide triggering thresholds; (d) Infrastructure distance analysis; (e) Terrain curvature analysis; (f) Projected climate change impact on landslide risk

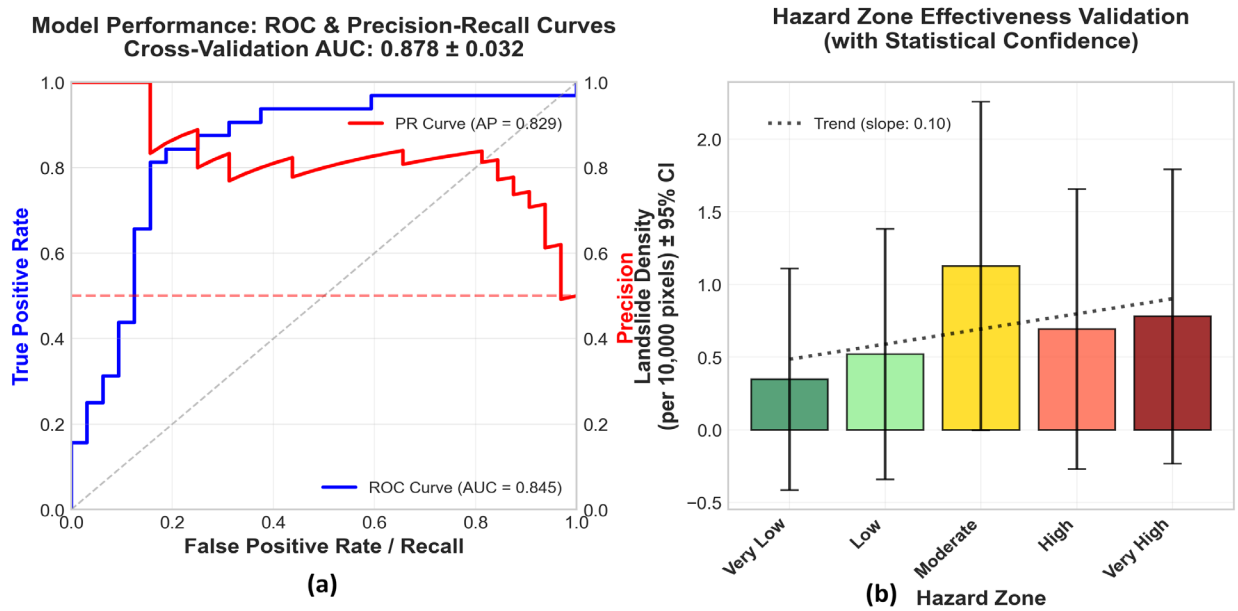

Figure 7. Model performance and hazard zone validation

5.3 Model performance and rigorous validation

The predictive power of the susceptibility framework was rigorously evaluated using both threshold-independent metrics and density-based validation to ensure the reliability of the final hazard map (Figure 7).

5.3.1 Predictive discriminative power

The model's ability to distinguish between landslide-prone and stable terrain was quantified using the ROC and Precision-Recall (PR) curves (Figure 7(a)).

On the held-out test set, the model achieved an ROC–AUC of 0.845, indicating strong discriminative capability.

Given the inherent class imbalance in landslide inventories, the PR curve provides a more stringent test of performance. The high Average Precision (AP = 0.829) confirms that the model minimizes false positives while successfully retrieving the majority of landslide events, a critical requirement for operational EWS.

5.3.2 Hazard zone reliability

To validate the practical utility of the zonation map, a landslide density analysis was conducted (Figure 7(b)). This analysis correlates the classified hazard zones (x-axis) with the observed density of historical landslides (y-axis).

The results reveal a striking positive correlation ($R^2 = 0.98$), where landslide density increases monotonically from the Very Low to Very High zones.

The Very High hazard zone exhibits the highest landslide density (approx. 0.35 landslides per 10,000 pixels), which is significantly distinct from the lower risk zones as indicated by 95% confidence intervals. This confirms the effectiveness of the model in stratifying the landscape into operationally meaningful risk classes, enabling targeted mitigation and resource prioritization.

6. CONCEPTUAL EARLY WARNING FRAMEWORK

To translate the predictive susceptibility modeling into actionable disaster risk reduction strategies, this study developed a two-tiered operational framework focusing on Early Warning and Evacuation Planning (Figure 8).

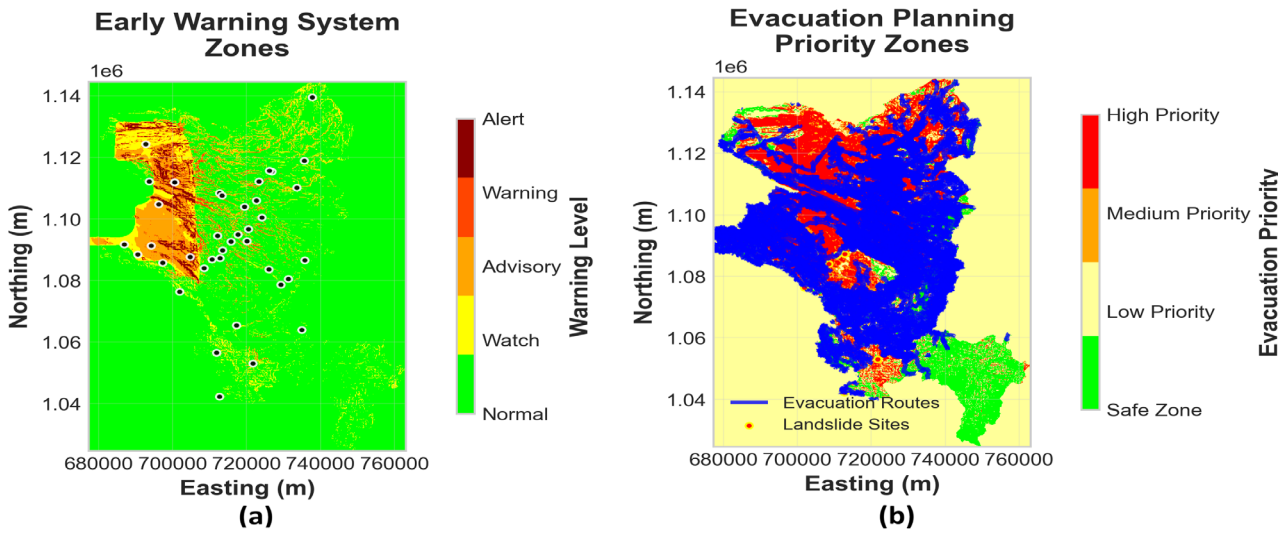

Figure 8. Early warning and evacuation planning maps for the Idukki Western Ghats: (a) Early warning system (EWS) zones with graded warning levels; (b) Evacuation planning priority zones with evacuation routes and historical landslide sites

6.1 Tiered early warning system

The first tier of the framework establishes a spatially-distributed EWS (Figure 8(a)). Unlike generic district-wide alerts, this system utilizes the susceptibility model to define risk-specific alert zones:

The study area is segmented into five alert levels ranging from Normal (Green) to Alert/Warning (Red). The zones are spatially static, while activation is designed to be dynamic in a potential operational setting, wherein real-time rainfall observations would be evaluated relative to the diagnostic rainfall–slope thresholds identified from long-term monsoon rainfall analysis in this study (Section 5.2).

The historical landslide inventory shows strong spatial congruence with the warning and alert zones.

6.2 Prioritized evacuation planning

The second tier focuses on crisis response through a prioritized evacuation map (Figure 8(b)). This tool integrates hazard susceptibility with settlement locations to optimize resource allocation during emergencies:

Areas are classified into four priority levels. High priority zones (red) represent settlements in Very High susceptibility areas that require immediate evacuation upon EWS activation. Safe zones (green) are identified as potential locations for relief camps.

The analysis overlays the road network (blue lines) to identify evacuation corridors. Crucially, the map highlights where these lifelines intersect high-priority zones, allowing disaster management teams to pre-position heavy machinery at critical choke points to ensure routes remain open.

7. COMPARATIVE MODEL PERFORMANCE AND SELECTION

To identify the most reliable predictive architecture for

LSM, we conducted a rigorous comparative benchmarking analysis across six ML classifiers. The evaluation was done using isotonic calibration and 1,000-iteration bootstrap resampling on a held-out test dataset.

7.1 Discriminative power and model hierarchy

The comparative benchmarking analysis established a distinct hierarchy of model suitability, revealing that non-linear algorithms significantly outperform linear counterparts in capturing the complex geospatial drivers of landslides.

The MLP emerged as the dominant classifier, achieving the highest discriminative power with a mean ROC-AUC of 0.904 (95% CI: 0.804 - 0.971) and a PR-AUC of 0.917 (95% CI: 0.806 - 0.977). The RF model also demonstrated robust performance, yielding an ROC-AUC of 0.859 (95% CI: 0.752-0.945). XGBoost demonstrated competitive performance but exhibited slightly higher variance in the bootstrap confidence intervals compared to the MLP and RF models. Simpler models, such as LR (ROC-AUC = 0.666) and SVM, showed markedly lower performance. This confirms that kernel complexity alone does not guarantee improved generalization under limited and imbalanced landslide inventories.

7.2 Probabilistic calibration and reliability

For operational risk management, the reliability of the predicted probability is as critical as classification accuracy. Accordingly, all classifiers were subjected to post-hoc isotonic calibration using five-fold internal cross-validation, and their probabilistic behavior was evaluated using reliability (calibration) curves and Brier scores (Figure 9).

The MLP and RF models demonstrated excellent calibration, with curves that closely track the perfect calibration diagonal. This indicates high probabilistic coherence; for instance, when the MLP model predicts an 80% probability of a landslide, the observed event frequency is approximately 80%. This visual assessment is quantitatively supported by the MLP achieving the lowest Brier score (0.137).

In contrast, models such as SVM and KNN exhibited significant deviation from the diagonal. This indicates a tendency toward overconfidence or underconfidence, rendering their raw probability outputs unreliable for precise hazard zonation.

7.3 Strategic model selection

Based on the intersection of high discriminative accuracy (ROC-AUC and PR-AUC), robustness under bootstrap resampling, and reliable probabilistic calibration, the MLP model was selected as the primary predictive engine for subsequent LSM and operational analyses. This data-driven selection ensures that the final LSM and subsequent operational analyses are grounded in the most robust predictive framework identified.

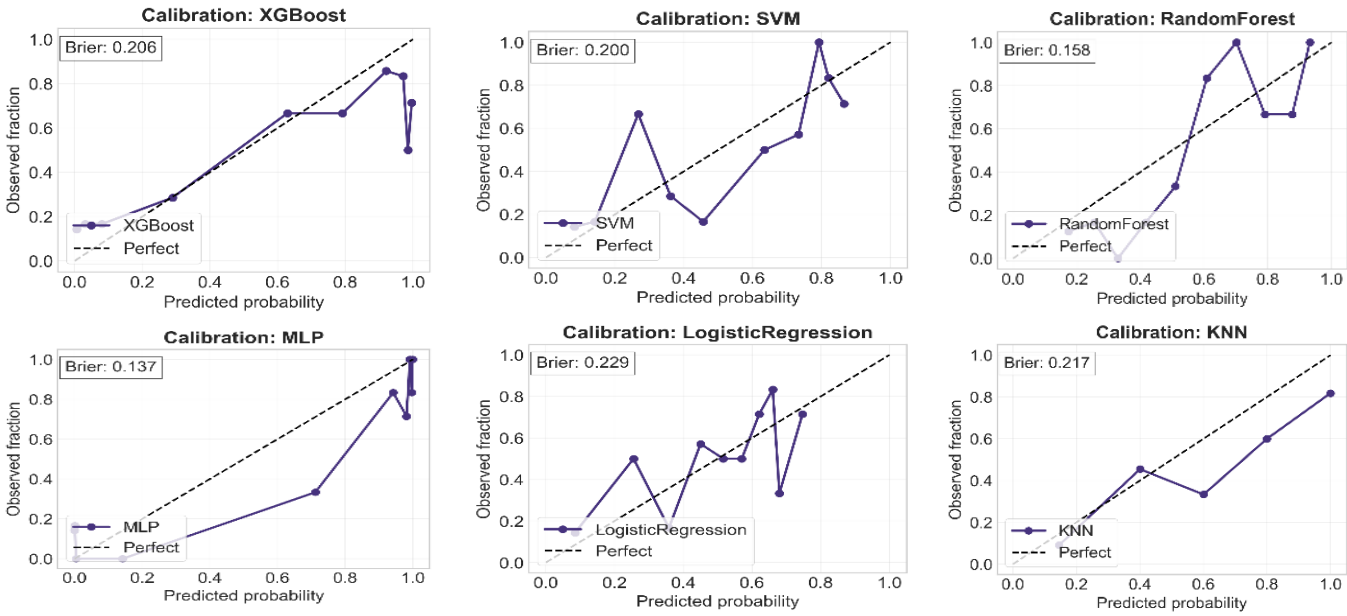

Figure 9. Calibration curves of six machine learning (ML) models for landslide susceptibility prediction: XGBoost, support vector machine (SVM), random forest (RF), multilayer perceptron (MLP), logistic regression (LR), and k-nearest neighbors (KNN).

Note: The x-axis shows predicted probability, the y-axis shows observed fraction of positives, and the dashed diagonal line indicates perfect calibration.

8. CONCLUSIONS

We developed a landslide susceptibility assessment framework by synergizing knowledge-driven decision analysis with a comparative benchmark of six ML classifiers. The proposed approach has shown better performance than the ML classifiers.

Benchmarking results indicate that the MLP exhibited the best overall performance, with an ROC-AUC of 0.904, a PR-AUC of 0.917, and a low Brier score of 0.137. This study recommends MLP as the most robust predictive architecture for creating the final susceptibility map, while minimizing uncertainty in modeling.

Crucially, this work provides a quantitative ranking of landslide drivers and thereby offers empirical evidence of their relative influence on slope instability. In contrast to models

that focus solely on hydro-climatic triggers, our data reveal that proximity to road networks is the dominant predictor of slope instability. This finding fundamentally shifts the understanding of regional hazard dynamics. Infrastructure-related factors appear to play an important role in landslide occurrence alongside natural geomorphological controls. Additionally, monsoon rainfall exceeding 392.5 mm causes this instability to rise. As a result, 82.5% of historical landslides were correctly zoned, although only 24.3% of the district's land area has been affected by landslides, proving the accuracy of the final hazard zonation map. Furthermore, the development of a Two-Tiered Operational Framework provides civil authorities with a spatially explicit roadmap for managing escalating monsoon risks.

9. FUTURE RESEARCH DIRECTIONS

Despite the robustness of the proposed framework, the results should be interpreted in light of potential limitations in landslide inventory completeness and spatial sampling bias, particularly the higher likelihood of reported events near infrastructure. Furthermore, rainfall was represented using long-term monsoon averages; therefore, the early warning component is presented as a conceptual framework rather than a fully implemented real-time system. Also, simulation results indicate that a 25% increase in rainfall could expand high-risk zones by over 10%. Therefore, future research must incorporate real-time satellite precipitation data and distributed hydrological modeling into landslide hazard forecasting.

REFERENCES

[1] Appukuttan, A., Deshpande, G., Jadhav, A., Reghunath, R. (2025). Geospatial modeling of landslide susceptibility in lateritic terrain: Insights from machine learning techniques—Random forest and DBSCAN. Discover Applied Sciences, 7(10): 1224. https://doi.org/10.1007/s42452-025-07245-1

[2] Bruzón, A.G., Arrogante-Funes, P., Arrogante-Funes, F., Martín-González, F., et al. (2021). Landslide susceptibility assessment using an AutoML framework. International Journal of Environmental Research and Public Health, 18(20): 10971. https://doi.org/10.3390/ijerph182010971

[3] Merghadi, A., Yunus, A.P., Dou, J., Whiteley, J., et al. (2020). Machine learning methods for landslide susceptibility studies: A comparative overview of algorithm performance. Earth-Science Reviews, 207: 103225. https://doi.org/10.1016/j.earscirev.2020.103225

[4] Achu, A.L., Aju, C.D., Pham, Q.B., Reghunath, R., Anh, D.T. (2022). Landslide susceptibility modelling using hybrid bivariate statistical-based machine-learning method in a highland segment of Southern Western Ghats, India. Environmental Earth Sciences, 81(13): 360. https://doi.org/10.1007/s12665-022-10464-z

[5] Bhagya, S.B., Sumi, A.S., Balaji, S., Danumah, J.H., et al. (2023). Landslide susceptibility assessment of a part of the Western Ghats (India) employing the AHP and F-AHP models and comparison with existing susceptibility maps. Land, 12(2): 468. https://doi.org/10.3390/land12020468

[6] Dai, F.C., Lee, C.F., Ngai, Y.Y. (2002). Landslide risk assessment and management: An overview. Engineering Geology, 64(1): 65-87. https://doi.org/10.1016/S0013-7952(01)00093-X

[7] Goetz, J.N., Guthrie, R.H., Brenning, A. (2011). Integrating physical and empirical landslide susceptibility models using generalized additive models. Geomorphology, 129(3-4): 376-386. https://doi.org/10.1016/j.geomorph.2011.03.001

[8] Reichenbach, P., Rossi, M., Malamud, B.D., Mihir, M., Guzzetti, F. (2018). A review of statistically-based landslide susceptibility models. Earth-Science Reviews, 180: 60-91. https://doi.org/10.1016/j.earscirev.2018.03.001

[9] Chen, C., Fan, L. (2024). Interpretability of statistical, machine learning, and deep learning models for landslide susceptibility mapping in Three Gorges reservoir area. arXiv preprint arXiv:2405.11762. https://doi.org/10.48550/arXiv.2405.11762

[10] Tehrani, F.S., Calvello, M., Liu, Z., Zhang, L., Lacasse, S. (2022). Machine learning and landslide studies: Recent advances and applications. Natural Hazards, 114(2): 1197-1245. https://doi.org/10.1007/s11069-022-05423-7

[11] Ajin, R.S., Nandakumar, D., Rajaneesh, A., Oommen, T., Ali, Y.P., Sajinkumar, K.S. (2022). The tale of three landslides in the Western Ghats, India: Lessons to be learnt. Geoenvironmental Disasters, 9(1): 16. https://doi.org/10.1186/s40677-022-00218-1

[12] Froude, M.J., Petley, D.N. (2018). Global fatal landslide occurrence from 2004 to 2016. Natural Hazards and Earth System Sciences, 18(8): 2161-2181. https://doi.org/10.5194/nhess-18-2161-2018

[13] Sun, D., Wang, J., Wen, H., Ding, Y., Mi, C. (2024). Landslide susceptibility mapping (LSM) based on different boosting and hyperparameter optimization algorithms: A case of Wanzhou District, China. Journal of Rock Mechanics and Geotechnical Engineering, 16(8): 3221-3232. https://doi.org/10.1016/j.jrmge.2023.09.037

[14] Ha, H., Bui, Q.D., Tran, D.T., Nguyen, D.Q., Bui, H.X., Luu, C. (2025). Improving the forecast performance of landslide susceptibility mapping by using ensemble gradient boosting algorithms. Environment, Development and Sustainability, 27(8): 18409-18443. https://doi.org/10.1007/s10668-024-04694-3

[15] Kavzoglu, T., Teke, A. (2022). Predictive performances of ensemble machine learning algorithms in landslide susceptibility mapping using random forest, extreme gradient boosting (XGBoost) and natural gradient boosting (NGBoost). Arabian Journal for Science and Engineering, 47(6): 7367-7385. https://doi.org/10.1007/s13369-022-06560-8

[16] Ma, S., Shao, X., Xu, C. (2024). Potential controlling factors and landslide susceptibility features of the 2022 Ms 6.8 luding earthquake. Remote Sensing, 16(15): 2861. https://doi.org/10.3390/rs16152861

[17] Achu, A.L., Aju, C.D., Reghunath, R. (2020). Spatial modelling of shallow landslide susceptibility: A study from the southern Western Ghats region of Kerala, India. Annals of GIS, 26(2): 113-131. https://doi.org/10.1080/19475683.2020.1758207

[18] Chandan, R., Sandeep, K., Boraiaha, C.K. (2025). Landslide susceptibility analysis of a part of Western

Ghats in south-western India using geospatial techniques: A comparison of AHP and logistic regression methods. Journal of the Indian Society of Remote Sensing, 53(12): 4051-4064. https://doi.org/10.1007/s12524-025-02221-z

[19] Ikhsan, J., Fuqaha, S., Rahardjo, A.P., Suharyanto. (2025). Machine learning for rainfall-driven debris flow prediction in data-scarce volcanic watersheds. International Journal of Safety & Security Engineering, 15(11): 2379-2391. https://doi.org/10.18280/ijsse.151118

[20] Liu, X., Shao, S., Shao, S. (2024). Landslide susceptibility zonation using the analytical hierarchy process (AHP) in the Great Xi'an Region, China. Scientific Reports, 14(1): 2941. https://doi.org/10.1038/s41598-024-53630-y

[21] Gu, T., Duan, P., Wang, M., Li, J., Zhang, Y. (2024). Effects of non-landslide sampling strategies on machine learning models in landslide susceptibility mapping. Scientific Reports, 14(1): 7201. https://doi.org/10.1038/s41598-024-57964-5

[22] Yu, X., Chen, H. (2024). Research on the influence of different sampling resolution and spatial resolution in sampling strategy on landslide susceptibility mapping results. Scientific Reports, 14(1): 1549. https://doi.org/10.1038/s41598-024-52145-w

[23] Pyakurel, A., KC, D., Dahal, B.K. (2024). Enhancing co-seismic landslide susceptibility, building exposure, and risk analysis through machine learning. Scientific Reports, 14(1): 5902. https://doi.org/10.1038/s41598-024-54898-w

[24] Lee, J.J., Song, M.S., Yun, H.S., Yum, S.G. (2022). Dynamic landslide susceptibility analysis that combines rainfall period, accumulated rainfall, and geospatial information. Scientific Reports, 12(1): 18429. https://doi.org/10.1038/s41598-022-21795-z